

## Ultrafast Transient Holographic Microscopy

Matz Liebel,\* Franco V. A. Camargo, Giulio Cerullo, and Niek F. van Hulst\*

Cite This: *Nano Lett.* 2021, 21, 1666–1671

Read Online

ACCESS |

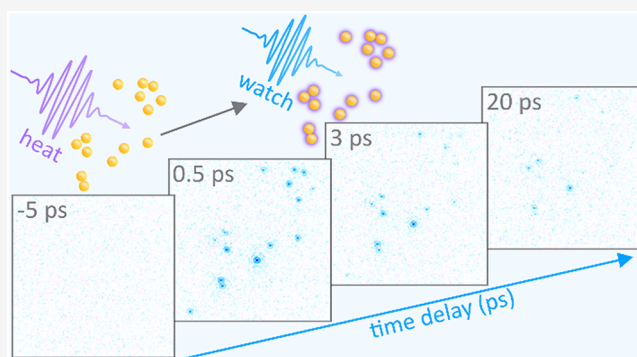
Metrics &amp; More

Article Recommendations

Supporting Information

**ABSTRACT:** Nanotechnology is increasingly being applied in many emerging technologies, ranging from metamaterials to next-generation nanodrugs. A key ingredient for its success is the ability to specifically tailor ultrafast nanoscale light–matter interactions over very large areas. Unfortunately, dynamic imaging by ultrafast nanoscopy so far remains limited to very small 2D areas. This shortcoming prevents connecting single-particle observations with large-scale functionality. Here, we address this experimental challenge by combining concepts of ultrafast spectroscopy, wide-field nanoscopy, and digital holography. We introduce an ultrafast holographic transient microscope for wide-field transient nanoscale imaging with high frequency all-optical signal demodulation. We simultaneously record ultrafast transient dynamics of many individual nano-objects and demonstrate time-resolved spectroscopy of gold nanoparticles over a large volume irrespective of their  $x$ – $y$ – $z$  position. Our results pave the way to single-shot 3D microscopy of 2D and 3D materials on arbitrary time scales from femtosecond carrier dynamics in optoelectronic materials to millisecond dynamics in complex tissues.

**KEYWORDS:** Holography, photothermal microscopy, transient absorption imaging, ultrafast dynamics, plasmonics, nanoparticles



Ultrafast nanoscopy is an emerging technology for studying transient phenomena on subwavelength scales<sup>1–6</sup> such as energy flow in semiconductor devices or the spectro-temporal dynamics of single nanoparticles and even single molecules.<sup>7–9</sup> Despite these advances, observations remain limited to very small 2D areas, which hinders single-shot capture of spatiotemporal images or the acquisition of sufficiently large data sets that allow quantifying the heterogeneous nature of many nanomaterials. As such, ultrafast studies of novel materials to visualize, for example, the temporal switching of metamaterials<sup>10</sup> or quantify light–matter interactions in strongly coupled systems<sup>11</sup> remain challenging to implement. Additionally, experiments addressing spatially more complex phenomena such as visualizing carrier diffusion in 3D<sup>12</sup> or quantifying the uptake and photoinduced heating of theranostic agents in tissue<sup>9,13</sup> are currently near-impossible to implement. Ideally, large field-of-view 3D transient nanoscopy would alleviate these limitations but requires high-frequency signal demodulation, which is currently incompatible with the typical frame rates of 2D cameras.

Here, we implement an all-optical ultrafast holographic transient (UHT) lock-in microscope that allows signal demodulation at arbitrary frequencies, independent of the camera frame rate. We demonstrate its broad applicability by simultaneously imaging dozens of individual gold nanoparticles (NPs) with diameters ranging from 20 to 100 nm, and simultaneously following their transient dynamics. We furthermore show that UHT microscopy is capable of computa-

tionally refocusing out-of-focus particles, thus paving the way toward 3D localization microspectroscopy over large volumes of view.

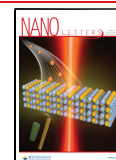
Figure 1a schematically depicts an experimental implementation of the UHT microscope, which can be conceptually separated into imaging and interference subsections. The former consists of collinear pump and probe pulses illuminating the sample and a dark-field microscope that images the sample-scattering onto a CMOS camera (Methods). As in a conventional transient absorption experiment, a chopper modulates the pump and the probe interrogates the sample in the presence and absence of photoexcitation as a function of pump–probe time delay.

The UHT microscope relies on multiplexed off-axis holography<sup>14–16</sup> to avoid restricting the pump modulation frequency to half the camera frame rate<sup>17</sup> and allow simultaneous recording of both pumped and unpumped images in a single camera exposure (Figure 1a). We generate suitable reference waves for the holographic experiment by diffracting a fraction of the probe pulse with a 2D  $0$ – $\pi$  phase grating and relay-image two of the first diffraction orders onto the camera, where

Received: November 6, 2020

Revised: January 27, 2021

Published: February 4, 2021



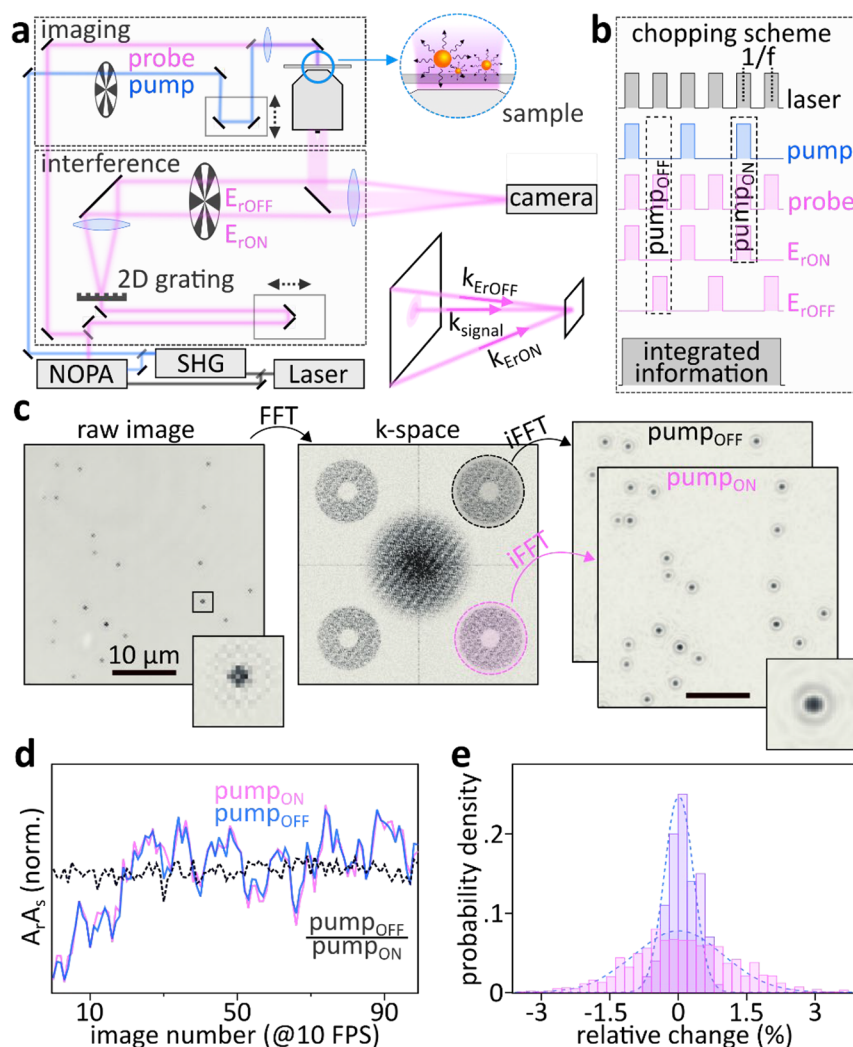


**Figure 1.** UHT microscope: an all-optical lock-in camera. (a) Experimental implementation of UHT microscopy with transient pump-delayed-probe imaging, and interference with modulated reference beams, allowing all-optical lock-in wide-field imaging on a camera. SHG, second harmonic generation; NOPA, noncollinear optical parametric amplifier. (b) Chopping scheme employed,  $1/f = 1$  ms is the time between individual laser pulses with  $f$  being the repetition rate of the laser system. (c) Data-processing workflow allowing retrieval of the scattering images for the pumped and unpumped sample by Fourier filtering in  $k$ -space. (d) Fluctuations of the radius of the  $\text{pump}_{\text{OFF}}$  (blue) and  $\text{pump}_{\text{ON}}$  (pink) interference signals, recorded at 10 frames-per-second (FPS), alongside their ratio (black, dashed). (e) Relative  $\text{pump}_{\text{OFF}}/\text{pump}_{\text{ON}}$  signal fluctuations recorded at 100 FPS (pink) and 10 FPS (purple) compared to shot-noise distributions (blue dashed lines) exhibiting  $10^4$  and  $10^5$  photons, respectively.

they interfere with the sample scattering (Methods).<sup>16,18,19</sup> A mechanical chopper, placed in the Fourier plane of the relay-imaging system, ensures that one diffraction order illuminates the camera when the pump is blocked and the other when the pump illuminates the sample (Figure 1a,b). This experimental implementation allows separating  $\text{pump}_{\text{OFF}}$  and  $\text{pump}_{\text{ON}}$  images in a holographic postprocessing step,<sup>16,20</sup> as can be understood by considering the total signal acquired on the camera,  $I_{\text{image}}$

$$I_{\text{image}} = |E_{r\text{OFF}}|^2 + |E_{r\text{ON}}|^2 + |E_{s\text{OFF}}|^2 + |E_{s\text{ON}}|^2 + E_{r\text{OFF}}^* E_{s\text{OFF}} + E_{r\text{ON}}^* E_{s\text{ON}} + \text{c. c.}$$

where  $E_{r\text{OFF}}$  and  $E_{r\text{ON}}$  are the electric fields of the reference waves in the absence and presence of the pump pulse and  $E_{s\text{OFF}}$  and  $E_{s\text{ON}}$  are the corresponding signal waves; c.c. stands for complex conjugate. As indicated in Figure 1a,  $E_{r\text{ON}}$  and  $E_{r\text{OFF}}$  exhibit different wavevectors thus moving the interference terms,  $E_{r\text{OFF}}^* E_{s\text{OFF}} + E_{r\text{ON}}^* E_{s\text{ON}} + \text{c.c.}$ , to distinct positions in momentum-space.<sup>21</sup> They are hence easily accessible via a

spatial Fourier transformation of the raw image, which reveals the diagonally shifted interference terms reminiscent of the microscope's back-focal-plane with the dark-field stop being visible in its center covering approximately one-third of the radius (Figure 1c, Supporting Information and Methods). Fourier-filtering<sup>20</sup> is hence sufficient to isolate the images acquired in the presence and absence of the pump. The simultaneous recording of  $\text{pump}_{\text{ON}}$  and  $\text{pump}_{\text{OFF}}$  images for consecutive pulses in a single exposure, furthermore, allows removing strongly correlated fluctuations by dividing the two (Figure 1d), and enables transient imaging near the shot-noise limit (Figure 1e). Our UHT microscope thus acts as an all-optical wide-field lock-in camera, which allows selecting arbitrary modulation frequencies and signal integration times with only the latter being determined by the camera exposure time. Compared to traditional lock-in amplifier-based demodulation approaches in a point-scanning configuration,<sup>3,4</sup> UHT microscopy directly demodulates entire 2D images, but crucially relies on the coherent nature of the signal of interest.

To demonstrate the capability of UHT microscopy to record temporally-resolved wide-field dynamics, we perform experiments on a sample composed of many individual 100 nm diameter gold NPs. Figure 2a shows an image acquired with a

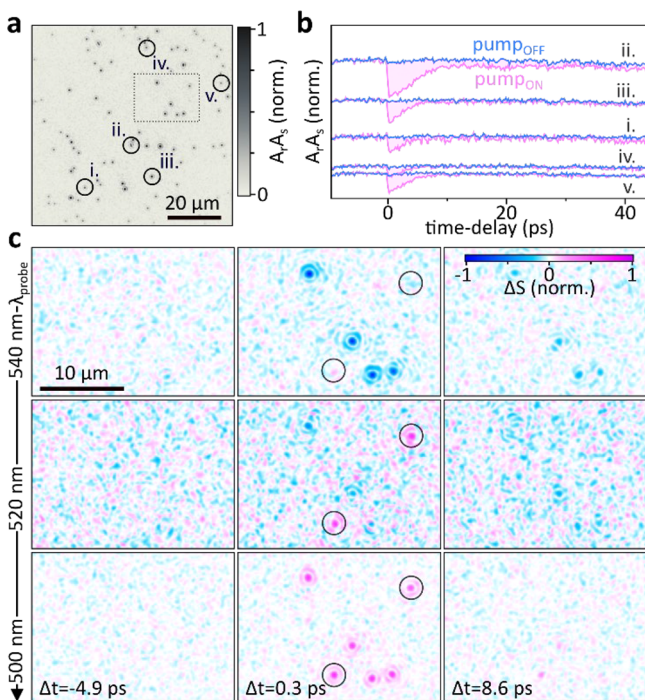


**Figure 2.** Wide-field transient imaging of single nanoparticles. (a) Pump<sub>OFF</sub> image of individual 100 nm Au-NPs. (b) Time-delay dependent scattering signal magnitudes at a probe wavelength of 540 nm for the five individual particles encircled in (a) recorded in the presence (pink) and absence (blue) of the 400 nm pump pulse with a fluence of 1.1 mJ/cm<sup>2</sup>. (c) Transient images within the dashed-rectangle in (a) for three different probe wavelengths as a function of pump–probe delay. From 540 to 500 nm, the NP transient-contrast inverts from negative to positive; note the black circles highlighting some NPs with signal-scaling that are considerably different from the average behavior (see Supporting Information for transient images of the entire field-of-view).

540 nm probe pulse, where the diffraction-limited spots are due to scattering of individual NPs. A 400 nm pump pulse photoexcites the NPs and we simultaneously record pump<sub>OFF</sub> and pump<sub>ON</sub> images as a function of pump–probe delay as outlined above. These image stacks allow accessing the transient dynamics of all individual NPs simultaneously by comparing their integrated scattering signal in the absence and presence of the pump (Figure 2b). At negative time delays, we observe nearly identical scattering signals, followed by a considerable pump<sub>ON</sub> signal decrease at positive delays rising within the ~200 fs instrumental response function. The transient signal shows the typical picosecond cooling dynamics of metallic nanoparticles due to thermalization of the hot electron distribution with the phonon bath.<sup>2,22,23</sup>

When tuning the probe wavelength from 540 to 500 nm across the spectral region of the localized surface plasmon resonance (LSPR),<sup>23,24</sup> we observe a sign inversion of the transient signal, computed as  $\Delta S(t) = A_{\text{rON}}A_{\text{sON}}(t) - A_{\text{rOFF}}A_{\text{sOFF}}(t)$ , where  $A_{\text{sON}}$  ( $A_{\text{sOFF}}$ ) and  $A_{\text{rON}}$  ( $A_{\text{rOFF}}$ ) are the electric field amplitudes of signal and reference waves, defined as  $E_j = A_j e^{-i\varphi_j}$ , in the presence (absence) of the pump (Figure 2c

and Supplementary Figure 1). Importantly, we directly uncover subtle details beyond the ensemble picture, as individual particles show distinctly different behavior with widely varying signals, an observation that is especially pronounced at 520 nm.

Next, to fully resolve the spectro-temporal differences, we record wavelength-resolved UHT images by tuning the probe from 500 to 651 nm, while keeping the pump at 400 nm (Methods and Supplementary Figure 3 for additional experiments performed on 200 nm NPs). Figure 3a shows the time-

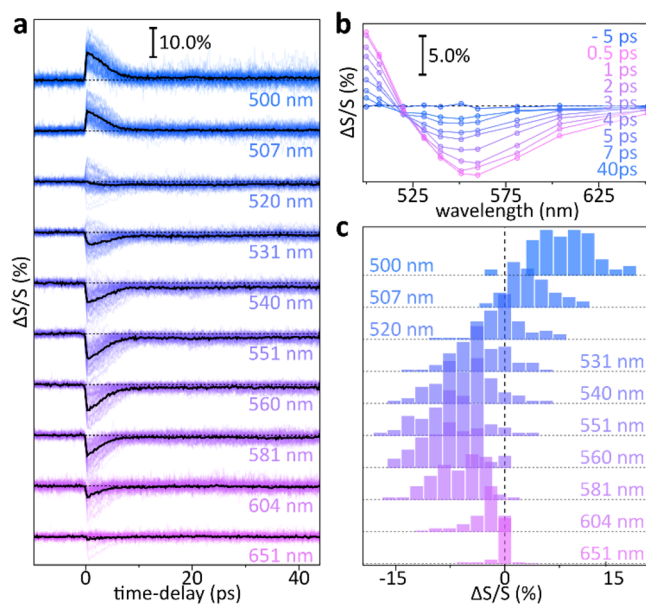


**Figure 3.** UHT imaging of single nanoparticle spectro-temporal dynamics. (a) Spectrally resolved transient dynamics of 76 individual 100 nm Au NPs (colored) alongside the mean dynamics (black). The transients are offset for clarity with the dashed line indicating  $\Delta S/S(t) = 0$  for the individual wavelengths. The wavelength dependent probe fluences are adjusted within the 0.1–0.4 mJ/cm<sup>2</sup> range and the pump fluence is 1.1 mJ/cm<sup>2</sup> (at  $1/e$ ). (b) Temporal representation of the decay dynamics of the averaged transient scattering spectra. (c) Histogram representation of the  $\Delta S/S(t)$  signal obtained by analyzing each individual NP in the 100–900 fs temporal window.

dependent transient scattering signal,  $\frac{\Delta S}{S}(t) = \frac{A_{\text{rON}}A_{\text{sON}}(t)}{A_{\text{rOFF}}A_{\text{sOFF}}(t)} - 1$ , for 76 simultaneously measured single NPs alongside their mean signal (Methods). The slight differences in decay kinetics (Figure 3a) are due to the varying pump fluence on the individual NPs, which results in different NP-heating and hence cooling dynamics, as verified by conducting additional measurements at different excitation fluences (Supplementary Figure 6).

Beyond the heating-induced differences, the 520–540 nm spectral region highlights the need for single-particle level spectroscopy as the mean signal fails to capture the widely differing transients. While the particle-averaged transient dynamics are a good estimate for the mean sample performance (Figure 3b), the underlying single-particle data paint a much more diverse picture (Figure 3c). Importantly, the histogram-spread is not due to experimental noise but a direct result of the size and shape heterogeneity of the NPs as well as their interaction with their specific nanoscopic environment.<sup>25</sup>

In line with previous experiments on gold NPs that predominantly monitored either transient absorption or transient extinction changes, we observe a broadening of the LSPR which results in a net bleach of the transition.<sup>26–28</sup> The

initially excited hot electron distribution rapidly thermalizes with the lattice phonons within a few picoseconds, resulting in bleach recovery. The residual  $\Delta S/S(t)$  signal at long delays (>40 ps) is due to the vibrationally hot NPs which slowly cool via NP-substrate coupling over time-scales far exceeding our experimental observation window.<sup>29</sup>

Having assessed the capability of UHT microscopy to perform wide-field transient imaging and spectroscopy, we evaluate the sensitivity of our method. The interferometric detection of the scattered field amplitude makes UHT microscopy particularly effective for detecting small NPs. To test the limits of recording wide-field transient NP dynamics we perform experiments while gradually reducing the particle diameter to 20 nm.

Figure 4a compares the holographically recorded scattering images of representative Au NPs of different sizes. As we reduce

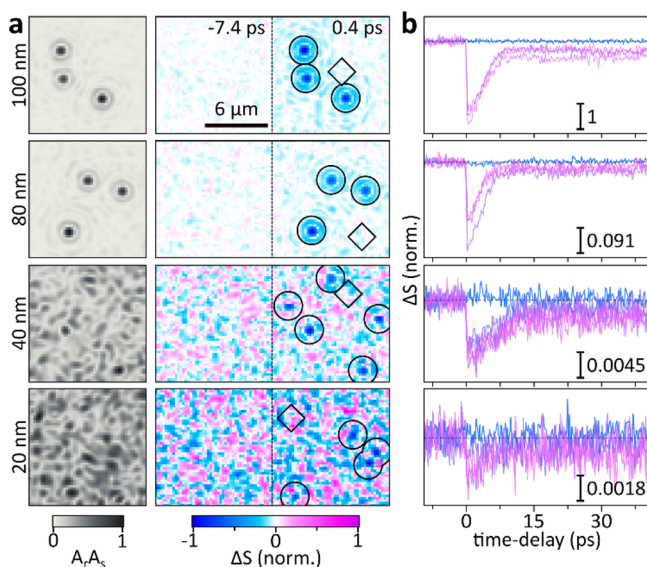


**Figure 4.** Signal scaling for different particle sizes. (a) Holographic (left) and transient scattering images (right) recorded for NP-diameters ranging from 100 to 20 nm using a 400 nm pump and a 540 nm probe pulse (see Methods for fluences). Circles indicate NPs, diamonds indicate a representative background region. (b) Time-traces of the particles highlighted in (a); the scale-bar indicates the relative scattering signal normalized to both pump intensity and probe amplitude. Blue lines indicate signals obtained at a background region and pink lines indicate signals due to NPs.

the particle size it becomes increasingly difficult to distinguish NP scattering and background. For 20 nm NPs, recorded in wide-field transmission geometry with a spatially coherent light source, both image contributions are essentially identical thus rendering the confident identification of the Au NPs with a standard holographic microscope as difficult to impossible. However, UHT microscopy is capable of recording transient images over a wide range of NP sizes (Figure 4a,b) that could even be boosted by approximately 1 order of magnitude by exchanging our NA = 0.5 objective for a higher NA oil-immersion objective.

Thus far, we have concentrated on spectroscopic and sensitivity aspects of UHT microscopy and ignored its holographic imaging capabilities. Beyond enabling wide-field lock-in detection, off-axis holography interferometrically measures both amplitude and phase information of an image. This direct access to the full electric field allows digital image

processing, such as computational focusing postacquisition, which enables 3D particle localization over large volumes-of-view from a single image.<sup>30</sup> Figure 5a shows the typical

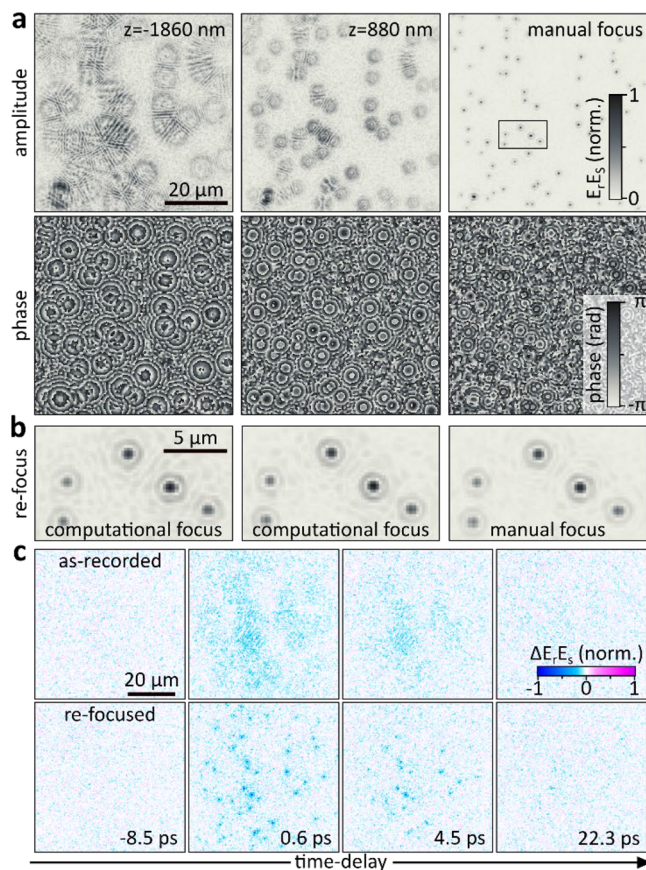


**Figure 5.** Digital refocusing of out-of-focus nanoparticles. (a) Scattering amplitude and phase of 100 nm Au NPs imaged below (left), above (center) and approximately in (right) the focal plane. (b) Representative images of the digitally refocused particles. (c) Transient wide-field-dynamics for the as-recorded, -1860 nm out-of-focus, image (top) as well as the refocused image obtained by computational back-propagation into focus (bottom).

information obtained from a hologram, processed as outlined previously (Figure 1c), for a sample containing 100 nm Au NPs placed at different relative distances with respect to the focal plane. The defocused NPs show the expected point-spread-function reminiscent of the imaging system used but the phase term reveals additional information. Depending on the precise location of the individual NPs with respect to the focal plane, we observe different amounts of spherical phase as well as a curvature inversion as we move through the focus.

We computationally refocus the out-of-focus images with the angular spectrum method<sup>21,31</sup> (Methods) and obtain near-identical images, irrespective of whether the particles are imaged near or far away from the image plane (Figure 5b). The same approach can be applied to UHT microscopy, allowing transient imaging and 3D localization of out-of-focus particles. Figure 5c validates this statement by comparing transient scattering images, recorded -1860 nm out-of-focus, of a 100 nm Au NP-sample with their refocused versions. While we see signs of the transient signal in the as-recorded image, the digitally refocused transient images show clear NP signatures comparable to the previously presented in-focus experiments (Figures 2–4).

Importantly, while we purposely chose a small defocus value of less than  $2\ \mu\text{m}$ , to allow visual identification of the individual NPs in the image, even  $>30\ \mu\text{m}$  defocused images are easily propagated back into focus.<sup>30,32</sup>

To summarize, we implemented a novel holographic transient, or UHT, microscope that allows performing wide-field pump–probe imaging. The platform yields complex images, comprised of both amplitude and phase terms, in a lock-in amplifier-like fashion irrespective of the camera's integration time. We demonstrated the platform's viability by simultaneously recording the spectro-temporally resolved transient dynamics of several tens of gold NPs with diameters as small as 20 nm and single-particle sensitivity. We deliberately chose the well-established gold NP system to allow direct intraplatform comparison with, for example, photothermal microscopes to aid the rapid adoption of the UHT technology by interested researchers. Beyond the NPs' dynamics, the simultaneously recorded phase information allows digital image propagation, thus paving the way toward recording transient dynamics of complex 3D samples and potentially transient absorption tomography. These advances are an important step toward highly multiplexed 3D transient absorption microscopy and will enable rationalizing structure–function relationships beyond 2D projections. Additionally, our results are highly relevant for single-particle tracking applications where background and photobleaching-free imaging methodologies are highly sought after. Especially for live cell and tissue imaging, our transient single-shot wide-field alternative to traditional point-scanning<sup>33,34</sup> photothermal microscopy eliminates the unfavorable temperature loss to the high heat-capacity solvent water and will allow real-time background-free imaging of intracellular processes over arbitrary observation times.

## METHODS

**UHT Microscope.** Spectrally tunable pulses are generated by a home-built noncollinear optical parametric amplifier (NOPA), pumped by a 1 kHz, 100 fs amplified Ti:sapphire laser, as described previously.<sup>35</sup> The 400 nm pump-pulse is directly obtained by frequency doubling the laser output. A 90:10 beam splitter generates the probe and the reference from the NOPA output. The former is made collinear with the pump-pulse and focused onto the sample by means of a  $F = 200$  mm achromatic lens. A home-built transmission dark-field microscope (NA = 0.5, Olympus RMS20X-PF), equipped with a dark-field mask in proximity of its back-focal-plane and a 488 nm long-pass filter (488 nm EdgeBasic, Semrock), images the sample scattering onto a CMOS camera (acA2040-90um Basler ace, Basler AG) at a nominal magnification of  $37\times$ . To allow holographic imaging we propagate the 10% probe-fraction through a relay-imaging system (nominal magnification  $0.5\times$ ) onto the same CMOS camera and place a 2D  $0-\pi$  phase grating (25.6 grooves/mm) into the conjugate image plane to allow interference over the entire camera chip.<sup>19</sup> We block all but two of the four first diffraction orders and modulate these two by means of a mechanical chopper thus separating  $\text{pump}_{\text{OFF}}$  and  $\text{pump}_{\text{ON}}$  interference terms as described in detail in the main text. The time-delay between signal and reference pulses is adjusted by maximizing the fringe contrast with a mechanical delay line. Pump–probe time-delay dependent images are recorded by means of a computer-controlled translation stage (M-531.PD1, Physik Instrumente).

**Sample Preparation.** A cover glass (#1.5) is cleaned by 10 min sonication in acetone, 10 min sonication in Milli-Q water,

drying under a stream of  $\text{N}_2$ , followed by a 5 min oxygen plasma treatment (Femto, Diener electronic GmbH). The cleaned glass is then incubated with PLL-g-PEG (SuSoS AG) for approximately 10 min, followed by a dilute Au NP-solution with the diameter of choice (citrate capped 20, 40, 80, 100, 200 nm all BBI Solutions). Once the NPs are bound, the residual solution is removed and the substrate is used for the optical experiments. Prior to performing UHT experiments, we characterized all samples using a k-scope which is capable of accurately sizing Au NPs in the 20–250 nm size-range.<sup>36</sup>

**Experimental Parameters.** Unless stated differently, the pump/probe fluences throughout the manuscript are given as  $1/\epsilon$  values. For the experiments presented in Figure 4, the fluences are the following: 100 nm NPs, 1.03 mJ/cm<sup>2</sup> pump, 0.15 mJ/cm<sup>2</sup> probe; 80 nm NPs, 1.74 mJ/cm<sup>2</sup> pump, 0.39 mJ/cm<sup>2</sup> probe; 40 and 20 nm NPs, 1.74 mJ/cm<sup>2</sup> pump, 1.59 mJ/cm<sup>2</sup> probe.

**Angular Spectrum Method.** We perform image-propagation via the angular spectrum method.<sup>21</sup> Briefly, the processed  $N \times N$  holograms are convolved with a propagation kernel of the form

$$K(x, y, z) = \exp(iz\sqrt{k_m^2 - k_x^2 - k_y^2})$$

where  $k_m = 2n\pi/\lambda$ , with  $n = 1$  being the refractive index of air. The discretized spatial frequencies are  $(k_x, k_y) = 2\pi/n\Delta x(x, y)$  for  $(-N/2 \leq x, y < N/2)$  with  $\Delta x$  representing the magnified pixel size of the imaging system.

**$\Delta S/S(t)$  and  $\Delta S$ .** Because of the dark-field nature of the UHT microscope, image regions without particles exhibit amplitudes close to zero. As a result, the intuitive differential scattering expression,  $\frac{\Delta S}{S}(t) = \frac{A_{\text{ON}}A_{\text{SON}}(t)}{A_{\text{OFF}}A_{\text{SOFF}}(t)} - 1$ , which reports on the relative scattering signal change due to photoexcitation, cannot be computed for images as for many points  $A_{\text{OFF}}A_{\text{SOFF}} \sim 0$ . To nevertheless show UHT images we employ the signal differences,  $\Delta S(t) = A_{\text{ON}}A_{\text{SON}}(t) - A_{\text{OFF}}A_{\text{SOFF}}(t)$  when images are reported where  $A_{\text{OFF}}A_{\text{SOFF}}(t)$  is often close to zero in regions where no particles are present.

## ASSOCIATED CONTENT

### Supporting Information

The Supporting Information is available free of charge at <https://pubs.acs.org/doi/10.1021/acs.nanolett.0c04416>.

Expanded version of Figure 2, information regarding the data processing of the holograms, additional experiments performed on 200 nm Au NPs, pump-fluence dependent measurements as well as pump and probe spectra (PDF)

## AUTHOR INFORMATION

### Corresponding Authors

Niek F. van Hulst – ICFO - Institut de Ciències Fotoniques, The Barcelona Institute of Science and Technology, 08860 Barcelona, Spain; ICREA - Institució Catalana de Recerca i Estudis Avançats, 08010 Barcelona, Spain; [orcid.org/0000-0003-4630-1776](https://orcid.org/0000-0003-4630-1776); Email: [niek.vanhulst@icfo.eu](mailto:niek.vanhulst@icfo.eu)

Matz Liebel – ICFO - Institut de Ciències Fotoniques, The Barcelona Institute of Science and Technology, 08860 Barcelona, Spain; [orcid.org/0000-0001-6220-3143](https://orcid.org/0000-0001-6220-3143); Email: [matz.liebel@icfo.eu](mailto:matz.liebel@icfo.eu)

### Authors

Franco V. A. Camargo – IFN-CNR, Dipartimento di Fisica, Politecnico di Milano, 20133 Milano, Italy

Giulio Cerullo – IFN-CNR, Dipartimento di Fisica, Politecnico di Milano, 20133 Milano, Italy; [orcid.org/0000-0002-9534-2702](https://orcid.org/0000-0002-9534-2702)

Complete contact information is available at:  
<https://pubs.acs.org/10.1021/acs.nanolett.0c04416>

## Notes

The authors declare no competing financial interest.

## ACKNOWLEDGMENTS

Authors acknowledge support by the Spanish Ministry of Science, Innovation, and Universities (MCIU/AEI: RTI2018-099957-J-I00 and PGC2018-096875-B-I00), the Ministry of Science and Innovations (MICINN “Severo Ochoa” program for Centers of Excellence in R&D CEX2019-000910-S), the Catalan AGAUR (2017SGR1369), Fundació Privada Cellex, Fundació Privada Mir-Puig, and the Generalitat de Catalunya through the CERCA program. N.F.v.H. acknowledges the financial support by the European Commission (ERC Advanced Grant 670949-LightNet). G.C. acknowledges support by the European Union Horizon 2020 Programme under Grant Agreement 881603 Graphene Core 3.

## REFERENCES

- (1) Schnedermann, C.; et al. Ultrafast Tracking of Exciton and Charge Carrier Transport in Optoelectronic Materials on the Nanometer Scale. *J. Phys. Chem. Lett.* **2019**, *10*, 6727–6733.
- (2) Block, A.; et al. Tracking ultrafast hot-electron diffusion in space and time by ultrafast thermomodulation microscopy. *Sci. Adv.* **2019**, *5*, No. eaav8965.
- (3) Huang, L.; Cheng, J.-X. Nonlinear Optical Microscopy of Single Nanostructures. *Annu. Rev. Mater. Res.* **2013**, *43*, 213–236.
- (4) Lo, S. S.; Devadas, M. S.; Major, T. a.; Hartland, G. V. Optical detection of single nano-objects by transient absorption microscopy. *Analyst* **2013**, *138*, 25–31.
- (5) Huber, B.; et al. Space- And time-resolved UV-to-NIR surface spectroscopy and 2D nanoscopy at 1 MHz repetition rate. *Rev. Sci. Instrum.* **2019**, *90*, 113103.
- (6) Denk, O.; Zheng, K.; Zigmantas, D.; Židek, K. Compressive imaging of transient absorption dynamics on the femtosecond timescale. *Opt. Express* **2019**, *27*, 10234.
- (7) Liebel, M.; Toninelli, C.; van Hulst, N. F. Room-temperature ultrafast nonlinear spectroscopy of a single molecule. *Nat. Photonics* **2018**, *12*, 45–49.
- (8) Guo, Z.; et al. Long-range hot-carrier transport in hybrid perovskites visualized by ultrafast microscopy. *Science (Washington, DC, U. S.)* **2017**, *356*, 59–62.
- (9) Delor, M.; Weaver, H. L.; Yu, Q. Q.; Ginsberg, N. S. Imaging material functionality through three-dimensional nanoscale tracking of energy flow. *Nat. Mater.* **2020**, *19*, 56–62.
- (10) Shaltout, A. M.; Shalaev, V. M.; Brongersma, M. L. Spatiotemporal light control with active metasurfaces. *Science (Washington, DC, U. S.)* **2019**, *364*, eaat3100.
- (11) Chikkaraddy, R.; et al. Single-molecule strong coupling at room temperature in plasmonic nanocavities. *Nature* **2016**, *535*, 127–130.
- (12) Ginsberg, N. S.; Tisdale, W. A. Spatially resolved photogenerated exciton and charge transport in emerging semiconductors. *Annu. Rev. Phys. Chem.* **2020**, *71*, 1–30.
- (13) Lim, E.-K.; et al. Nanomaterials for Theranostics: Recent Advances and Future Challenges. *Chem. Rev.* **2015**, *115*, 327–394.
- (14) Kühn, J.; et al. Real-time dual-wavelength digital holographic microscopy with a single hologram acquisition. *Opt. Express* **2007**, *15*, 7231–7242.
- (15) Colomb, T.; et al. Polarization microscopy by use of digital holography: Application to optical-fiber birefringence measurements. *Appl. Opt.* **2005**, *44*, 4461–4469.
- (16) Rubin, M.; Dardikman, G.; Mirsky, S. K.; Turko, N. A.; Shaked, N. T. Six-pack off-axis holography. *Opt. Lett.* **2017**, *42*, 4611–4614.
- (17) Schnedermann, C.; et al. Sub-10 fs Time-Resolved Vibronic Optical Microscopy. *J. Phys. Chem. Lett.* **2016**, *7*, 4854–4859.
- (18) Bon, P.; Maucort, G.; Wattellier, B.; Monneret, S. Quadriwave lateral shearing interferometry for quantitative phase microscopy of living cells. *Opt. Express* **2009**, *17*, 13080–13094.
- (19) Maznev, A. A.; Crimmins, T. F.; Nelson, K. A. How to make femtosecond pulses overlap. *Opt. Lett.* **1998**, *23*, 1378–1380.
- (20) Takeda, M.; Ina, H.; Kobayashi, S. Fourier-transform method of fringe-pattern analysis for computer-based topography and interferometry. *J. Opt. Soc. Am.* **1982**, *72*, 156.
- (21) Goodman, J. W. *Introduction to Fourier optics*; W.H. Freeman & Co Ltd: New York, 2005.
- (22) Pelton, M.; Liu, M.; Park, S.; Scherer, N. F.; Guyot-Sionnest, P. Ultrafast resonant optical scattering from single gold nanorods: Large nonlinearities and plasmon saturation. *Phys. Rev. B: Condens. Matter Mater. Phys.* **2006**, *73*, 1–6.
- (23) Baida, H.; Mongin, D.; Christofilos, D.; Bachelier, G.; Crut, A.; Maioli, P.; Del Fatti, N.; Vallee, F. Ultrafast nonlinear optical response of a single gold nanorod near its surface plasmon resonance. *Phys. Rev. Lett.* **2011**, *107*, 1–5.
- (24) Itoh, T.; Asahi, T.; Masuhara, H. Femtosecond light scattering spectroscopy of single gold nanoparticles. *Appl. Phys. Lett.* **2001**, *79*, 1667–1669.
- (25) Piatkowski, L.; Gellings, E.; van Hulst, N. F. Broadband single-molecule excitation spectroscopy. *Nat. Commun.* **2016**, *7*, 10411.
- (26) Voisin, C.; Del Fatti, N.; Christofilos, D.; Vallee, F. Ultrafast electron dynamics and optical nonlinearities in metal nanoparticles. *J. Phys. Chem. B* **2001**, *105*, 2264–2280.
- (27) Hodak, J. H.; Henglein, A.; Hartland, G. V. Photophysics of nanometer sized metal particles: Electron-phonon coupling and coherent excitation of breathing vibrational modes. *J. Phys. Chem. B* **2000**, *104*, 9954–9965.
- (28) Link, S.; El-Sayed, M. A. Optical Properties and Ultrafast Dynamics of Metallic Nanocrystals. *Annu. Rev. Phys. Chem.* **2003**, *54*, 331–366.
- (29) Baffou, G.; Quidant, R. Thermo-plasmonics: Using metallic nanostructures as nano-sources of heat. *Laser Photonics Rev.* **2013**, *7*, 171–187.
- (30) Memmolo, P.; et al. Recent advances in holographic 3D particle tracking. *Adv. Opt. Photonics* **2015**, *7*, 713–755.
- (31) Poon, T.-C.; Liu, J.-P. *Introduction to Modern Digital Holography with MATLAB*; Cambridge University Press: Cambridge, U.K., 2014.
- (32) Latychevskaia, T.; Fink, H.-W. Holographic time-resolved particle tracking by means of three-dimensional volumetric deconvolution. *Opt. Express* **2014**, *22*, 20994–21003.
- (33) Pache, C.; et al. Fast three-dimensional imaging of gold nanoparticles in living cells with photothermal optical lock-in Optical Coherence Microscopy. *Opt. Express* **2012**, *20*, 21385.
- (34) Lasne, D.; et al. Single Nanoparticle Photothermal Tracking (SNaPT) of 5-nm gold beads in live cells. *Biophys. J.* **2006**, *91*, 4598–4604.
- (35) Manzoni, C.; Polli, D.; Cerullo, G. Two-color pump-probe system broadly tunable over the visible and the near infrared with sub-30 fs temporal resolution. *Rev. Sci. Instrum.* **2006**, *77*, 023103.
- (36) Ortiz-Orruño, U.; Jo, A.; Lee, H.; van Hulst, N. F.; Liebel, M. Precise nanosizing with high dynamic range holography. *Nano Lett.* **2021**, *21*, 317–322.